RESULTS ON HARD DIFFRACTION FROM H1

T.R. EBERT
(for the H1 Collaboration)
Oliver Lodge Laboratory, University of Liverpool, Liverpool, U.K.

A measurement of the diffractive structure function $F_2^{D(3)}(\beta, Q^2, x_{I\!P})$ from the H1 experiment is presented. The $x_{I\!P}$ dependence of $F_2^{D(3)}$ is found to vary with β, demonstrating that the factorisation of a universal diffractive flux from the cross-section is not possible. The data are consistent with there being a contribution from both pomeron and meson exchange. The structure function of the exchange ($\tilde{F}_2^D(\beta, Q^2)$) shows scaling violations with Q^2, and a QCD fit leads to the conclusion that the momentum is carried largely by gluons. The properties of the hadronic final state in diffractive events are studied. Measurements of energy flow and charged particle, charm and jet production are presented. They are all consistent with the structure of the pomeron being dominated by gluons.

1 Introduction

Deep inelastic scattering events containing a large interval of rapidity without any hadronic activity (a "rapidity gap")[1,2] are interpreted as being dominantly diffractive in nature[3]. The hadronic final state of any event can be decomposed into two systems X and Y separated by the largest gap in rapidity and in the case of diffraction, the masses of both systems are small compared to the $\gamma^* p$ centre of mass energy (W).

In addition to the standard deep-inelastic variables Q^2, y and W^2, two variables are introduced:

$$\beta \simeq \frac{Q^2}{Q^2 + M_X^2} \qquad x_{I\!P} \simeq \frac{Q^2 + M_X^2}{Q^2 + W^2} \tag{1}$$

They have a simple interpretation in terms of an exchanged object (e.g. a pomeron); $x_{I\!P}$ is the fraction of the proton's momentum carried by the exchanged object and β is the fraction of the momentum of the exchanged object carried by the struck quark. The 4–momentum transfer squared at the proton vertex is t.

2 The Diffractive Structure Function

The analysis is based on $\sim 2\,\mathrm{pb}^{-1}$ data taken by the H1 experiment in 1994, and covers the kinematic range $2.5 < Q^2 < 65\,\mathrm{GeV}^2$, $0.01 < \beta < 0.9$ and $10^{-4} < x_{I\!P} < 0.05$. Experimentally, diffractive events with a system Y of low mass are selected on the basis of having no activity in a series of forward detectors in H1 [4], with sensitivity to the rapidity range $3.4 < \eta < 7.5$. The selection ensures that the system X is well contained in the detector and the system Y, which is not measured, has a mass $M_Y < 1.6\,\mathrm{GeV}$. The requirement $x_{I\!P} < 0.05$ means that Y carries more that 95% of the incident proton's momentum. The selection restricts t, which is not measured, to the range $\mid t \mid < 1\,\mathrm{GeV}^2$. The contribution to the event sample from events with proton dissociation is estimated to be $\sim 5\%$.

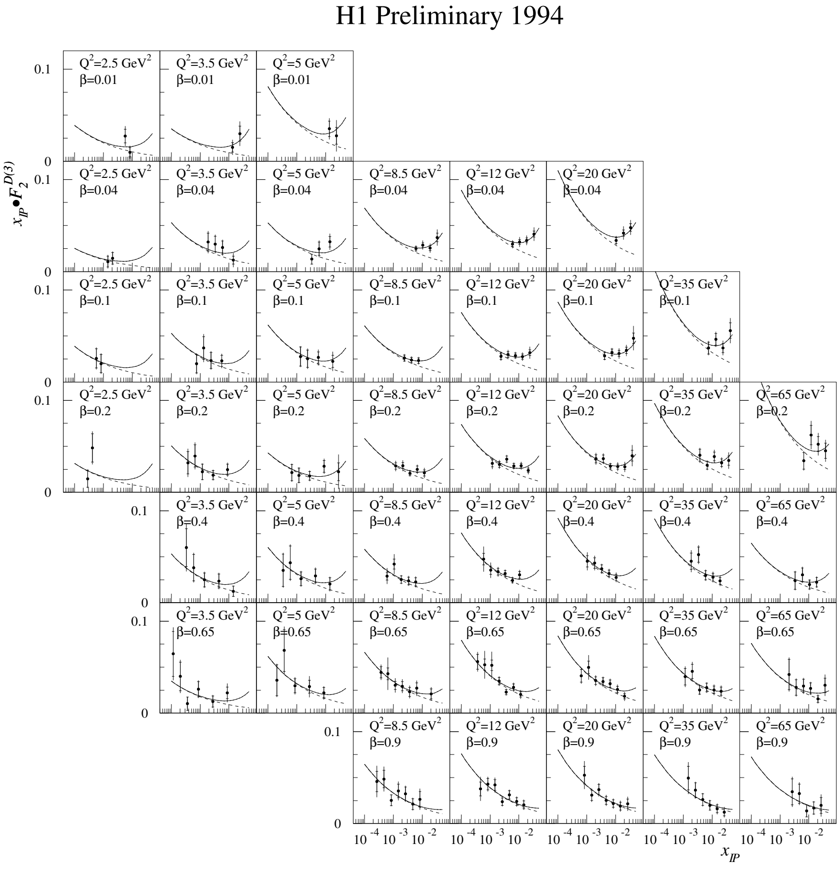

Figure 1: $x_{I\!P} \cdot F_2^{D(3)}(\beta, Q^2, x_{I\!P})$ as a function of $x_{I\!P}$ in bins of β and Q^2. A fit to the data (see text for details) including a pomeron and meson component (solid line) and the pomeron component to this (dashed line) are shown.

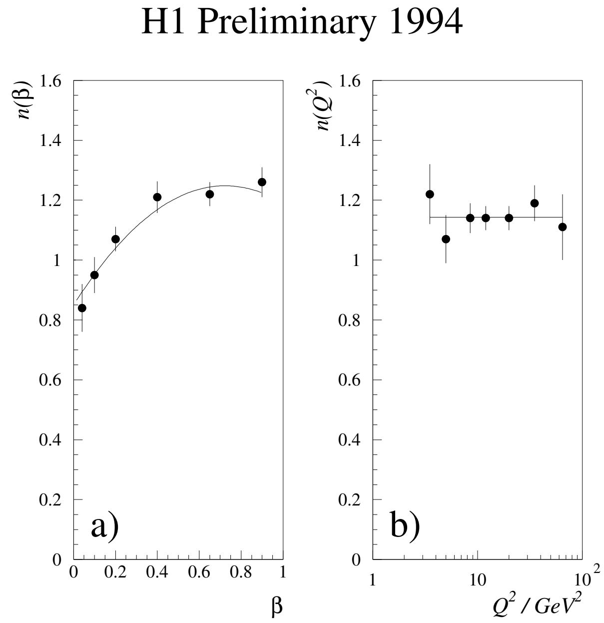

Figure 2: n from the fit $F_2^{D(3)} = A(\beta, Q^2) \cdot x_{I\!P}^{-n}$ where (a) $n = n(\beta)$ and (b) $n = n(Q^2)$.

The diffractive structure function $F_2^{D(3)}(\beta, Q^2, x_{I\!P})$ is defined as [5]:

$$\frac{\mathrm{d}^3\,\sigma^D_{ep\to e'XY}}{\mathrm{d}\beta\,\mathrm{d}Q^2\,\mathrm{d}x_{I\!P}} = \frac{4\pi\alpha^2}{\beta Q^4}(1 - y + \frac{y^2}{2})F_2^{D(3)}(\beta, Q^2, x_{I\!P}) \tag{2}$$

with the integral over the measured t range having been performed. Figure 1 shows $x_{I\!P} \cdot F_2^{D(3)}$ as a function of $x_{I\!P}$ for different values of β and Q^2.

A universal flux of pomerons associated with the proton implies that $F_2^{D(3)}$ can be factorised in the form $F_2^{D(3)} \propto x_{I\!P}^{-n}$ where n is $2\alpha(t) - 1$ averaged over the t dependence of the cross-section and $\alpha(t) = \alpha(0) + \alpha' t$ is the effective pomeron trajectory [6]. Figure 2 shows the resulting values of n from such a fit to the data, allowing n to vary with either β or Q^2. Whilst there is no evidence for a dependence on Q^2, n increases with increasing β. Therefore the factorisation of $F_2^{D(3)}$ into terms depending only on β and Q^2, with the $x_{I\!P}$ dependence describing a universal flux of pomerons is not valid.

The most probable explanation for this is a contribution from meson exchange (e.g. $f_2^0(1270)$). Figure 1 shows a phenomenological fit to $F_2^{D(3)}$ with a pomeron and a meson component:

$$F_2^{D(3)} = A^{I\!P}(\beta, Q^2) \cdot x_{I\!P}^{-n_{I\!P}} + C_M \cdot F_2^M(\beta, Q^2) \cdot x_{I\!P}^{-n_M} \qquad (3)$$

where $A^{I\!P}$ is proportional to the pomeron structure function. The GRV parameterisation of the pion structure function [7] is used for F_2^M and $A^{I\!P}$, $n_{I\!P}$, C_M and n_M are fitted simultaneously. This procedure gives an excellent fit to the data ($\chi^2/ndf = 165/156$) yielding $n_{I\!P} = 1.29 \pm 0.03(\mathrm{stat}) \pm 0.07(\mathrm{syst})$ and $n_M = 0.3 \pm 0.3(\mathrm{stat}) \pm 0.6(\mathrm{syst})$. The influence of a possible interference between the two components is included in the systematic error [9].

The integration over t is corrected for assuming a peripheral t dependence (e^{bt}) with $b_M = 5$ and $b_{I\!P} = 6$ and linear trajectories ($\alpha(t) = \alpha(0) + \alpha' t$) with $\alpha'_M = 1$ and $\alpha'_{I\!P} = 0.3$. This yields $\alpha(0)_M = 0.6 \pm 0.1(\mathrm{stat}) \pm 0.3(\mathrm{syst})$ and $\alpha(0)_{I\!P} = 1.18 \pm 0.02(\mathrm{stat}) \pm 0.04(\mathrm{syst})$.

3 The Partonic Structure of Diffractive Exchange

.

The structure function $\tilde{F}_2^D$:

$$\tilde{F}_2^D(\beta, Q^2) = \int_{x_{I\!P}=0.0003}^{x_{I\!P}=0.05} F_2^{D(3)}(\beta, Q^2, x_{I\!P}) dx_{I\!P} \qquad (4)$$

which is proportional to the average deep inelastic structure of the exchange, is shown in figure 3. At fixed Q^2, $\tilde{F}_2^D$ is consistent with being independent of β but scaling violations are clearly seen in the Q^2 dependence at fixed β. The conclusions are unaffected by the possible presence of meson exchange [9].

A QCD analysis of $\tilde{F}_2^D$ was performed. The $u + d + s$ quark distributions and the gluon distribution are parameterised at a scale $Q_0^2 = 2.5\,\mathrm{GeV}^2$ with the form $x \cdot f(x) = Ax^B(1-x)^C$ and evolved to higher Q^2 using DGLAP evolution. Charm is introduced via boson-gluon fusion [10], and no momentum sum-rule is applied [11].

Two possible solutions are considered; only quarks or both quarks and gluons are present at the starting scale. The resulting fits are shown in figure 4. The data requires a significant gluon density at the starting scale.

The parton densities obtained from the QCD fit with both quarks and gluons at the starting scale are shown in figure 5. Close to the starting scale, a "leading" gluon behaviour is seen, in which the exchange is dominated by gluons with fractional momentum $x_{g/I\!P} > 0.9$. Also shown is the integrated momentum fraction carried by quarks and gluons as a function of Q^2. Throughout the Q^2 range, gluons carry in excess of 80% of the momentum of the exchange.

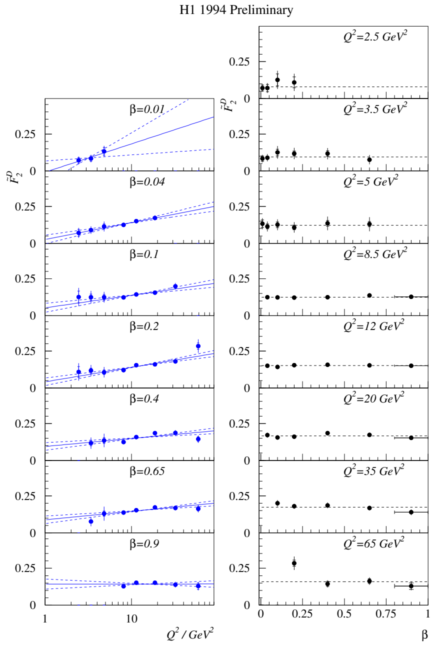

Figure 3: $\tilde{F}_2^D$ as a function of Q^2 for different values of β (left) and as a function of β for different values of Q^2 (right).

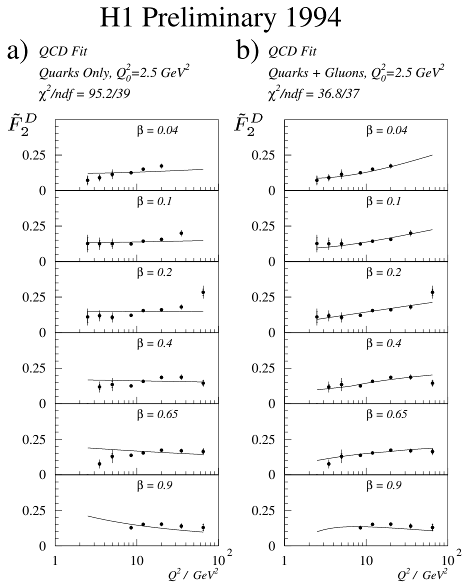

Figure 4: QCD fit to $\tilde{F}_2^D$ assuming (a) only quarks (b) both quarks and gluons at the starting scale of $Q_0^2 = 2.5\,\mathrm{GeV}^2$

4 The Hadronic Final State in Diffractive Events

The picture of diffractive deep inelastic scattering described above has consequences for the hadronic final state. If the pomeron is a quark dominated object, the leading order process is $eq \to eq$ with the exchanged photon coupling directly to a quark from the pomeron. The struck quark and pomeron remnant have small transverse momentum with respect to the $\gamma^* I\!P$ axis in the $\gamma^* I\!P$ centre-of-mass frame. However, for a gluon dominated pomeron, the leading order process is boson-gluon fusion, and the $q\bar{q}$ pair from the hard sub-process can have significant transverse momentum with respect to this axis.

For a gluon dominanted pomeron, therefore, more energy flow in the central region of the $\gamma^* I\!P$ system and increased high p_T particle production is expected. The thrust distribution will show a two jet configuration, and more di-jet events will be observed. The cross-section for charm production is also

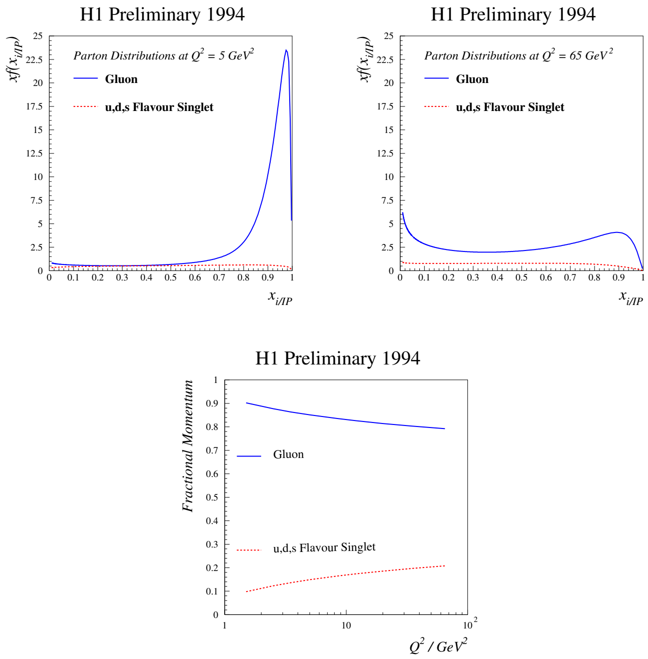

Figure 5: Parton densities from the fit to $\tilde{F}_2^D$ at (a) $Q^2 = 5\,\mathrm{GeV}^2$ and (b) $Q^2 = 65\,\mathrm{GeV}^2$ allowing both quarks and gluons at $Q_0^2 = 2.5\,\mathrm{GeV}^2$. The fraction of the total momentum carried by quarks and gluons as a function of Q^2 is shown in (c).

higher, as the boson-gluon fusion process is dominant.

The Monte Carlo generator RAPGAP [12] was used for comparison with the data. In this model, the pomeron has a partonic structure and the two sets of parton densities obtained from the QCD fit to $\tilde{F}_2^D$ under the assumption that the pomeron contains only quarks (the RG-Q model) or a mixture of quarks and gluons (the RG-QG model) at $Q^2 = 2.5\,\mathrm{GeV}^2$ were used. Two different models of QCD radiation were used for the RG-QG model – leading log parton showers (MEPS) and the colour dipole model (CDM). The RG-Q model uses the colour dipole model.

4.1 Energy Flow and Charged Particle Production

Details of the measurements can be found elsewhere [13]. Results are presented in the kinematic range $7.5 < Q^2 < 100\,\mathrm{GeV}^2$, $0.05 < y < 0.6$ and $x_{I\!P} < 0.025$.

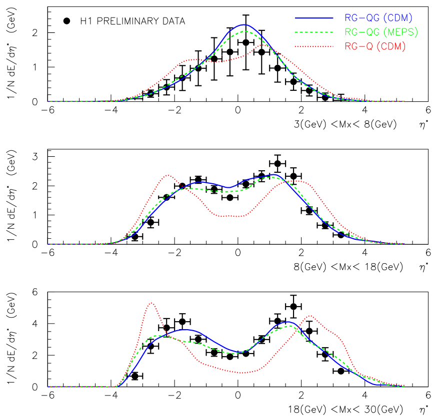

Figure 6: Energy flow in the $\gamma^* I\!\!P$ frame in ranges of M_X. The H1 data is compared to the RG-Q (dotted line) and RG-QG (solid and dashed lines) models.

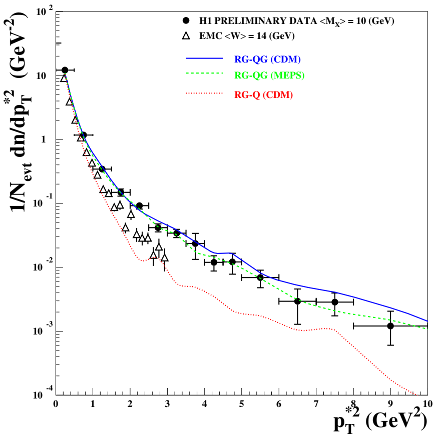

Figure 7: The p_T^{*2} distribution of charged particles. The H1 diffractive data in the $\gamma^* I\!\!P$ frame (black points) are compared to EMC μp data in the $\gamma^* p$ frame (white points). The RG-Q (dotted line) and RG-QG (solid and dashed lines) are also shown.

Figure 6 shows the energy flow as a function of pseudorapidity in the $\gamma^* I\!\!P$ frame, in bins of M_X. The data is compared to the RG-Q and RG-QG models. Whilst the RG-Q model significantly underestimates the energy flow at $\eta^* \approx 0$, the models which include the "leading gluon" parameterisation for the pomeron are able to describe the data.

The track p_T^{*2} distribution relative to the $\gamma^* I\!\!P$ axis is shown in figure 7. The H1 diffractive data ($< M_X >= 10\,\mathrm{GeV}$) in the $\gamma^* I\!\!P$ frame is compared to EMC deep–inelastic μp data ($< W >= 14\,\mathrm{GeV}$) [14] in the $\gamma^* p$ frame. There is an excess of high p_T^{*2} particles in the diffractive data over the EMC data. This presumably arises from the large contribution from boson gluon fusion in the diffractive events, as the EMC data is in a kinematic region where the proton structure is dominated by quarks. This is confirmed by the comparison with the models; whilst the RG-Q model lies below the data, the two RG-QG models are in good agreement with the measured data points.

The Feynman-x (x_F) distribution is shown in figure 8, with the H1 data again compared to EMC data. The EMC data is asymmetric about $x_F = 0$, which is consequence of the fact that unlike the struck parton, the proton remnant is an extended object. In contrast, for the H1 diffractive data the distribution is symmetric, implying a similarity between the struck parton and

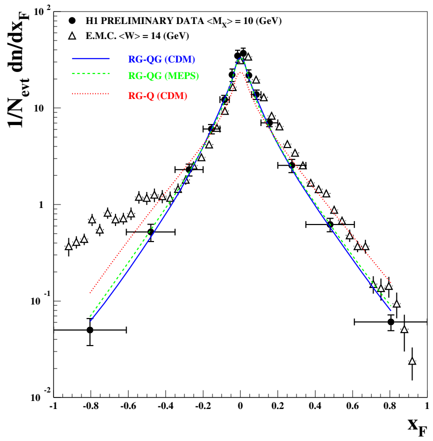

Figure 8: The x_F distribution showing H1 diffractive data in the $\gamma^* I\!P$ frame (black points) and EMC μp data in the $\gamma^* p$ frame (white points). The RG-Q (dotted line) and RG-QG (solid and dashed lines) are also shown.

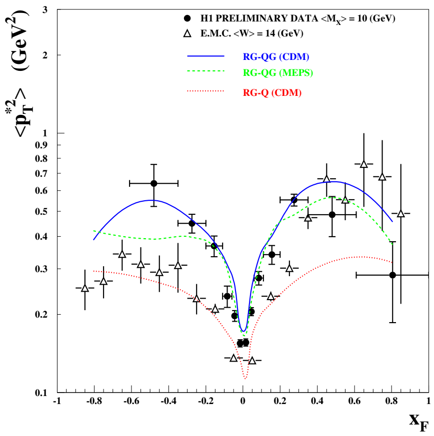

Figure 9: Seagull plot for H1 diffractive data in the $\gamma^* I\!P$ frame (black points) and EMC μp data in the $\gamma^* p$ frame (white points). The RG-Q (dotted line) and RG-QG (solid and dashed lines) are also shown.

the pomeron remnant. The data is again described by the RG-QG models.

Figure 9 shows the $< p_T^{*2} >$ as a function of x_F. The EMC data are asymmetric, with the $< p_T^{*2} >$ in the remnant hemisphere suppressed with respect to that in the struck parton hemisphere owing to the extended nature of the proton remnant [15]. In contrast, the H1 diffractive data are symmetric about $x_F = 0$, suggesting that the pomeron remnant is a compact object like the struck parton. The $<p_T^{*2}>$ at $x_F = 0$ is higher for the H1 data than the EMC data, indicating that more of the diffractive events involve a high p_T process. Again whilst the RG-Q model fails to describe the data, the RG-QG model gives a good description of the measured values.

4.2 Observation of Charm

$D^{*\pm}$ mesons are reconstructed via the decay $D^{*\pm} \to D^0\pi^\pm_{slow} \to (K^\mp\pi^\pm)\pi^\pm_{slow}$ [13]. The distribution of the mass difference between the $D^{*\pm}$ and D^0 candidates is shown in figure 10.

The cross-section for $D^{*\pm}$ production in the system X is measured to be:

$$\sigma(ep \to eD^*XY) = 380^{+150}_{-120}(\text{stat})^{+140}_{-110}(\text{syst})\,\text{pb}$$

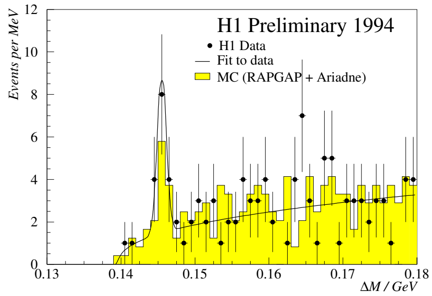

Figure 10: $\Delta\mathrm{M} = M(K\pi\pi_{slow}) - M(K\pi)$ for D^* candidates. H1 data are compared to the RG-QG model.

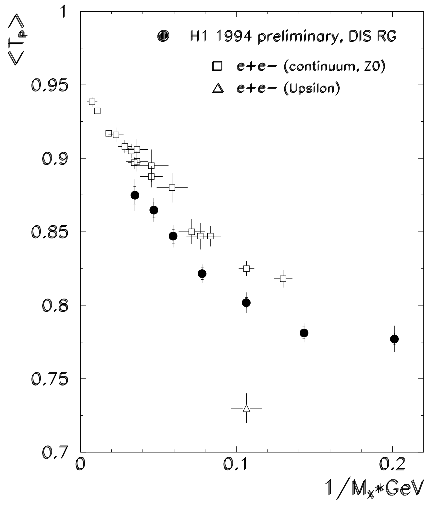

Figure 11: $<T>$ versus $1/M_x$ for H1 diffractive data (black points) and a selection of e^+e^- data (white points).

in the kinematic range $10 < Q^2 < 100\,\mathrm{GeV}^2$, $0.06 < y < 0.6$, $x_{I\!P} < 0.05$, $M_Y < 1.6\,\mathrm{GeV}$, $|\ \eta(D^*)\ | < 1.25$ and $p_T(D^*) > 1.0\,\mathrm{GeV}$. The RG-Q model predicts a cross-section of $\sim 10\,\mathrm{pb}^{-1}$ and the RG-QG model predicts a cross-section of $\sim 200\,\mathrm{pb}^{-1}$. The measured cross-section is inconsistent at the 2σ level with the prediction based on a quark dominated pomeron.

4.3 Thrust

In the centre of mass of a system of N particles, thrust is defined as:

$$T = \frac{1}{\sum_{i=1}^{N} |\vec{p}_i|} \times \max\left\{\Sigma_{i=1}^{N} |\vec{p}_i \cdot \vec{n}|\right\} \qquad (5)$$

and its value varies between 0.5 (isotropic event of infinite multiplicity) and 1.0 (two particles).

The $<T>$ for diffractive events is shown in figure 11 as a function of $1/M_X$. Details of this measurement can be found elsewhere[16]. The H1 diffractive data are compared to measurements from e^+e^- experiments. The results show that the diffractive events are basically two-jet like in nature, with the jets becoming more collimated with increasing M_X. More than $\sim 30\%$ of events have a thrust

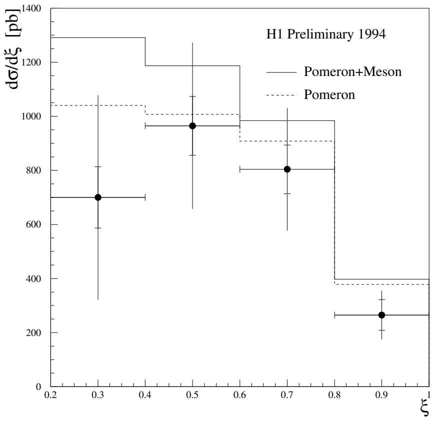

Figure 12: Differential di-jet cross-section in diffractive photoproduction. The data is compared to POMPYT with $I\!P$ (dashed line) and with meson and $I\!P$ (solid line) exchange, with $I\!P$ parton densities obtained from the fit to $F_2^{D(3)}$.

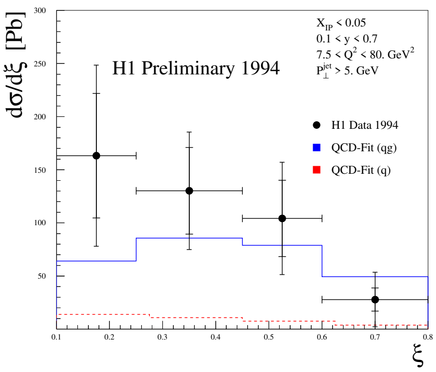

Figure 13: Differential di-jet cross-section for $7.5 < Q^2 < 80\,\mathrm{GeV}^2$. The solid line shows the prediction from the RG-QG model and the dashed line the prediction from the RG-Q model.

jet $p_T^2 > 3\,\mathrm{GeV}^2$. The $< T >$ is lower in the diffractive data than the e^+e^- measurements, indicating a higher parton multiplicity in the diffractive events.

4.4 High p_T Jets

Di-jet production has been studied in both diffractive photoproduction and diffractive deep-inelastic scattering.

The photoproduction analysis covers the kinematic range $10^{-8} < Q^2 < 0.01\,\mathrm{GeV}^2$ and $0.25 < y < 0.7$ and the deep inelastic data considers events with $7.5 < Q^2 < 100\,\mathrm{GeV}^2$ and $0.1 < y < 0.7$. In both cases, $x_{I\!P} < 0.05$. A cone algorithm is used to reconstruct jets in the $\gamma^* I\!P$ centre of mass frame, and at least two jets with $p_T > 5\,\mathrm{GeV}$ with respect to the photon direction are required.

The di-jet cross-section is presented as a function of ξ, which is a hadron level estimator of the momentum fraction of the exchanged object which enters the hard subprocess. ξ is reconstructed from the jets:

$$\xi_{\gamma p} = \frac{(E+P_z)_{jets}}{(E+P_z)_X}; \qquad \xi_{\gamma^* p} = \frac{Q^2 + M_{jj}^2}{Q^2 + M_X^2} \tag{6}$$

Figure 12 shows the differential di-jet cross-section $d\sigma/d\xi$ for the photoproduction data and the prediction from the POMPYT Monte Carlo [17], using the leading gluon parameterisation for the structure of the pomeron obtained from the QCD fit to $\tilde{F}_2^D$. The result of including a meson component is also shown. The model is in reasonable agreement with the data, thus supporting the hypothesis of a factorisable pomeron flux and a universal pomeron structure.

Figure 13 shows $d\sigma/d\xi$ for the deep-inelastic diffractive data. The di-jet cross-section from the RG-Q model is significantly below the measured values but the RG-QG model is able to give a reasonable description of the data.

5 Conclusions

A measurement of the diffractive structure function $F_2^{D(3)}(\beta, Q^2, x_{I\!P})$ has been presented. The data can be described by a superposition of pomeron and meson exchange. The structure function of the exchange ($\tilde{F}_2^D$) shows scaling violations with Q^2, and a QCD fit leads to the conclusion that the momentum of the exchange is carried largely by gluons.

Features of the hadronic final state are well reproduced by a model based on a flux of pomerons with parton densities obtained from the QCD fit to the inclusive measurement $\tilde{F}_2^D$. There is increased energy flow and high p_T^* particle, charm and jet production over the expectations from a model in which the pomeron structure is quark dominated.

Acknowledgements

I would like to thank the members of the H1 diffractive group for informative discussions on this material.

References

1. ZEUS Collaboration, Phys. Lett. **B315** (1993) 481.
2. H1 Collaboration, Nucl. Phys. **B429** (1994) 477.
3. H1 Collaboration, Phys. Lett. **B348** (1995) 681.
4. H1 Collaboration, Nucl. Instr. and Meth. **A386** (1997) 310 and **A386** (1997) 348.
5. G. Ingelman and P. Schlein, Phys. Lett. **B152** (1985) 256.
6. See for example P. Collins, "An Introduction to Regge Theory and High Energy Physics", Cambridge University Press, (1997)
7. M. Gluck, E. Reya, A. Vogt, Z. Phys. **C53** (1992) 651.

8. NMC Collaboration, Phys. Lett. **B364** (1995) 107.
BCDMS Collaboration, Phys. Lett. **B223** (1989) 485.
9. H1 Collaboration, "A Measurement and QCD Analysis of the Diffractive Structure Function $F_2^{D(3)}$", Proc. of ICHEP '96, Warsaw, July 1996.
10. H1 Collaboration, Nucl. Phys. **B470** (1996) 3.
11. L. Trentadue and G. Veneziano, Phys. Lett. **B323** (1994) 201.
12. H. Jung, Comp. Phys. Comm. **86** (1995) 147
13. C. Cormack, Thesis (University of Liverpool) in litt.
14. EMC Collaboration, Z. Phys. **C35** (1987) 417.
15. EMC Collaboration, Phys. Lett. **B149** (1984) 415.
16. H1 Collaboration, "Thrust Jet Analysis of Deep–Inelastic Large Rapidity Gap Events at HERA", Proc. of ICHEP '96, Warsaw, July 1996.
17. P. Bruni and G. Ingelman, Proc. Europhysics Conf. on HEP, Marseilles 1993, 595.